J. Fluid Mech. (1997), *vol.* 342, *pp.* 141–158. Printed in the United Kingdom

Reflection of a high-amplitude solitary wave at a vertical wall

By M. J. COOKER,[1] P. D. WEIDMAN[2] AND D. S. BALE[3]

[1] School of Mathematics, University of East Anglia, Norwich NR4 7TJ, UK

[2] Department of Mechanical Engineering, University of Colorado, Boulder, CO 80309, USA

[3] Department of Physics, University of Colorado, Boulder, CO 80309, USA

(Received 29 February 1996 and in revised form 25 October 1996)

The collision of a solitary wave, travelling over a horizontal bed, with a vertical wall is investigated using a boundary-integral method to compute the potential fluid flow described by the Euler equations. We concentrate on reporting new results for that part of the motion when the wave is near the wall. The wall residence time, i.e. the time the wave crest remains attached to the wall, is introduced. It is shown that the wall residence time provides an unambiguous characterization of the phase shift incurred during reflection for waves of both small and large amplitude. Numerically computed attachment and detachment times and amplitudes are compared with asymptotic formulae developed using the perturbation results of Su & Mirie (1980). Other features of the flow, including the maximum run-up and the instantaneous wall force, are also presented. The numerically determined residence times are in good agreement with measurements taken from a cine film of solitary wave reflection experiments conducted by Maxworthy (1976).

1. Introduction

In this paper we consider the reflection at a vertical wall of a solitary wave, using a boundary-integral numerical code, a perturbation method, and re-analysis of cine film taken during the study by Maxworthy (1976). Most attention is given to that part of the motion during which the point of greatest free-surface elevation (the crest) lies close to the wall.

The problem of solitary wave reflection has received attention in studies of the interaction between solitary waves, of which the head-on collision of two equal waves is a special case equivalent to that studied here. When weakly nonlinear solitary waves overtake or collide with one another there may be a spatial phase shift but no loss of energy from either wave once sufficient time has passed for the two waves to separate; this is the feature by which a *soliton* is defined (Zabusky & Kruskal 1965). Recent studies have shown that large-amplitude solitary water waves do not behave like solitons. A long time after the collision between two equal waves there is a loss to secondary waves, and a reduction in wave speed. The reduced wave speed necessarily produces a spatial phase shift that increases without bound as $t \to \infty$.

It is useful to briefly review certain aspects of the phenomena we wish to study, some of which bear on the interpretation of results to be presented later. In what follows, $\zeta(x, t)$ is the free-surface elevation about the quiescent fluid level and $\epsilon = a/h$ is the dimensionless solitary wave amplitude, a being the amplitude of the incident wave travelling on a fluid of constant still-water depth h. Byatt-Smith (1971) investigated the interaction between two weakly nonlinear solitary waves travelling in opposite

directions and explicitly determined the maximum amplitude of the collision. When, in the absence of viscosity and surface tension, two waves of equal amplitude collide, one has the problem of solitary wave reflection from a vertical wall. For this case the maximum elevation ζ_0 of the wave at the wall, the 'run-up,' was reported to be

$$\zeta_0/h = 2\epsilon + \tfrac{1}{2}\epsilon^2, \tag{1.1a}$$

showing that the run-up exceeds twice the amplitude of the incident solitary wave. Oikawa & Yajima (1973) explicitly computed the spatial phase shift ΔX incurred after reflection from the wall, namely

$$\Delta X/h = (\tfrac{1}{3}\epsilon)^{1/2}, \tag{1.1b}$$

and it was later noted (Weidman, cf. Maxworthy 1976) that this result is implicitly contained in the earlier solution of Byatt-Smith (1971). To test the above results, Maxworthy (1976) performed experiments in a wave tank 5 m long with still-water depths in the range $4.5 < h < 6.7$ cm, investigating both endwall and wave–wave collisions. Here we discuss only his endwall collisions. The solitary wave was initiated by judiciously varying the amplitude and velocity of a plate pulled through the tank far from the endwall, and amplitudes up to $\epsilon \approx 0.5$ were produced for endwall collision experiments. The motion was recorded on 64 frame/s cine film. Maxworthy found run-ups ζ_0 in qualitative agreement with (1.1*a*). However his measured phase shifts were, within experimental error, independent of ϵ with a reported value of $\Delta X/h \approx 1.2$ and thus the square-root dependence on ϵ was not verified; in fact his measurements ranged from 1 to 3 times the value given by (1.1*b*). (We have taken into account, as observed by Fenton & Rienecker (1982), that Maxworthy plotted twice the value of $\Delta X/h$ given in (1.1*b*) for comparison with experiment in his figure 3.) The wave crest lingers at the wall during reflection for a period which we denote t_r, the wall residence time. A noteworthy feature in figure 2 of Maxworthy (1976) is that immediately before and after impact with the wall the wave crest moves extremely quickly.

Following the experiment described above, there have been a number of developments starting with the work of Su & Mirie (1980, hereinafter abbreviated to SM), who carried out a perturbation analysis of two colliding solitary waves to $O(\epsilon^3)$. They found that, although a small dispersive tail trails behind the skewed (backward-tilting) wave after reflection from the wall, the wave recovers its shape and speed asymptotically so that its soliton nature is preserved. One concludes, therefore, that no energy is lost to the dispersive tail at this order in ϵ. The improved formulae for maximum run-up and phase shift found by SM are

$$\zeta_0/h = 2\epsilon + \tfrac{1}{2}\epsilon^2 + \tfrac{3}{4}\epsilon^3, \quad \Delta X/h = (\tfrac{1}{3}\epsilon)^{1/2}(1 + \tfrac{7}{8}\epsilon). \tag{1.2a, b}$$

Mirie & Su (1982) continued their study by numerically integrating the Su & Gardner (1969) equations and produced results for equal-amplitude solitary wave collision. They found the skewed reflected waveform and the small dispersive tail. However, the waves did not fully recover their original amplitude after head-on collision, the loss in amplitude being 0.2% for $\epsilon = 0.1$ increasing to 2% for $\epsilon = 0.5$.

Fenton & Rienecker (1982) used a Fourier series method to solve the fully nonlinear Euler equations. Their results for the run-up are in close agreement with the experimental results of Chan & Street (1970). They further showed that while the $O(\epsilon^3)$ theory of SM provides excellent results for the maximum run-up, the spatial phase shift depends strongly on the position from the wall at which it is measured. In view of this finding, they suggested that any experiments to determine a phase shift should be carried out at distances $x > 15h$ from the reflecting boundary. Renouard, Seabra-Santos & Temperville (1985) subsequently performed careful laboratory experiments

of solitary wave reflection. They found, in agreement with Mirie & Su (1982) and Fenton & Rienecker (1982), a transient loss of amplitude as the reflected wave propagates away from the wall. They placed their probes in the region $15 < x/h < 35$, an evident compromise between being sufficiently far from the wall to exceed the zone of amplitude recovery yet sufficiently close to avoid serious attenuation due to viscous damping. Their measured phase shifts are considerably smaller than those of Maxworthy (1976); however the scatter is so great that one cannot realistically discern if the data better fit (1.1*b*) or the improved perturbation result (1.2*b*). Renouard *et al.* (1985) conclude that the phase shift is highly sensitive to experimental conditions.

Byatt-Smith (1988) put the energy loss problem on firm ground by analytically investigating the equal-amplitude solitary wave collision to higher order than previously considered. He definitively shows that the change in amplitude asymptotically far from the collision plane is $O(\epsilon^5)$. The fact that energy loss first shows up at this high order explains why even moderate-amplitude solitary waves do closely exhibit soliton behaviour both in numerical computations and laboratory experiments.

Grilli & Svendsen (1990) use a boundary-integral method to solve for the potential flow beneath a moving free surface. Integrations are initiated with data for a solitary wave using the exact technique of Tanaka (1986). They show that for $\epsilon > 0.3$ the time evolution of the force on the wall has two extrema. The first and larger maximum occurs before the time of greatest run-up, here denoted by t_0, and the smaller second maximum in force occurs after t_0. This confirms the results of Cooker (1990) who used the boundary-integral method of Dold & Peregrine (1986), as adapted by Tanaka *et al.* (1987). Cooker (1990) reported results for waves up to $\epsilon = 0.7$ and concluded that the double force extrema on the wall is associated with the high vertical acceleration in the motion near the water line (see also Mirie & Su 1982). Cooker (1990) also computed estimates of the time the wave crest resides at the wall.

In this investigation we present results obtained using the fully nonlinear potential flow code of Cooker (1990) with exact solitary wave initial data computed by the method of Tanaka (1986). Realizing that soliton behaviour cannot persist after reflection at high amplitudes, we concentrate on the motion of the wave when it is near the wall, and obtain estimates of the wall force and the wall residence time, t_r. We propose that t_r be considered as a unified (in the sense that it encompasses both weakly nonlinear and high-amplitude waves) measure of the interaction phase changes, which is easily computed numerically, or measured experimentally.

In §2 we describe the numerical method used to solve the moving free boundary problem with potential flow. Section 3 gives asymptotic estimates of the times and amplitudes of wave attachment, detachment, and maximum run-up deduced from the available perturbation results of SM. In §4 numerical and asymptotic results characterizing the wall interaction process are compared. We further examine in §4 an original cine film of Maxworthy (1976) to extract measurements of the wall attachment and detachment times relative to the time at maximum run-up. A discussion of results and concluding remarks are given in §5.

2. Boundary-integral method

We briefly outline the method due to Dold & Peregrine (1986), as adapted by Tanaka *et al.* (1987) and see also Dold (1992). The technique follows the trend begun by Longuet-Higgins & Cokelet (1976), Vinje & Brevik (1981), and Baker, Meiron & Orszag (1982). The water is modelled as inviscid and incompressible fluid in irrotational motion with a free surface, F. Air motion and surface tension are neglected so that the dynamic boundary condition on F is that the fluid pressure is a constant

(zero). The still-water level lies at $y = 0$, and the horizontal impermeable bed lies at $y = -h$. The bed is treated as a line of symmetry of the solution. F is discretized with points which model fluid particles, obeying the kinematic boundary condition, that particles on F remain on F. The coordinates of a typical point on F are $[X(s, t), Y(s, t)]$ where s is a Lagrangian point-label parameter which increases monotonically along F and takes successive integer values at the discretization points. The velocity potential inside the fluid is $\phi(x, y, t)$. On F, at a point labelled by s, $\phi = \phi[X(s, t), Y(s, t)] \equiv \Phi(s, t)$. The potential is harmonic in the fluid domain, and on F we have the boundary conditions (for a fluid of unit density)

$$\mathrm{D}\Phi/\mathrm{D}t = \tfrac{1}{2}(u^2+v^2) - gY, \tag{2.1}$$

$$\mathrm{D}X/\mathrm{D}t = \partial\phi/\partial x, \tag{2.2}$$

$$\mathrm{D}Y/\mathrm{D}t = \partial\phi/\partial y. \tag{2.3}$$

The method works on a repeated cycle of three steps as follows:

(i) Stipulate values of X, Y, Φ at an initial instant t;

(ii) Solve a boundary-integral equation to find the velocity on F, and the acceleration, and higher time derivatives of position;

(iii) Apply (2.1)–(2.3) to time step (X, Y) to the new position of F and update Φ. This provides new data for step (i).

The boundary-integral equation in step (ii) is derived from Cauchy's integral in principle value form for the complex-conjugate velocity $U = u - \mathrm{i}v$. U is expressed in terms of components tangential and normal to F. The tangential velocity component is found immediately from the data along the free surface and the normal component is a function of s which satisfies the integral equation in step (ii). The integral equation is discretized and simplified to a set of linear equations. Due account is taken of the finite contributions to the integral from the singular points. Jacobi iteration is used to solve the system beginning with the solution at the previous time step as a good approximation for the first iterate. In step (iii) the time stepping is carried out by expanding X, Y, Φ as fifth-order Taylor series in time, the coefficients of these series contain terms which depend upon the solutions u, v (and their partial time derivatives) of the integral equation found in step (ii). The time step size is chosen to ensure that the last terms of the Taylor series are decreasing in absolute magnitude.

Although some or all of the above features are incorporated in boundary-integral methods, the Dold & Peregrine (1986) method utilizes techniques which make it more accurate and efficient than others. The fifth-order Taylor series in time ensures an accurate prescription of the trajectory of each fluid particle. Tangential derivatives are calculated with a tenth-order central difference formula, which gives much greater accuracy than for example cubic splines. For a fluid domain which is quiescent at infinity we can truncate the domain and allow it to expand as waves propagate toward the ends of the computational domain. The Jacobi iteration to solve the linear system from the integral equation is much more efficient, for a large number of surface discretization points, than a direct method for inverting the system.

As previously mentioned, the boundary-integral method is initiated with solitary wave data using the method of Tanaka (1986). This discretization places points closer together at the crest than in the tails of the waveform, with separation distance inversely proportional to the speed along F as measured in a frame of reference moving with the crest. The horizontal distance from the wave crest to the wall is x_0 which for each wave was chosen so that the fluid elevation at the wall was less than $10^{-5}h$. The method is efficient. A free surface composed of 200 points (for a solitary wave of height $\epsilon = 0.4$) can be simulated over a model time of 10τ (where $\tau = (h/g)^{1/2}$ in under 10

minutes on a Sun workstation. The accuracy of the code may be judged in results in tables 1 and 2 in §4; here the calculated phase speeds determined over the first 10 time steps, at selected values of ϵ, are compared with the corresponding exact values computed by the method of Tanaka (1986). Over the time intervals computed the mass of fluid above still-water level was conserved to within an error of less than 0.05%. As further testimony to the algorithm's accuracy the total energy was conserved to within an error of 0.006% of its initial value. These errors fluctuated through positive and negative values as the computations proceeded.

3. Perturbation results

3.1. *Wave attachment and detachment*

It is clear from the studies of Mirie & Su (1982), Fenton & Rienecker (1982), and Byatt-Smith (1988) that large-amplitude solitary waves lose energy on reflection from a vertical wall, and hence such waves cannot follow a uniformly shifted reflected phase trajectory. In figure 1 we depict a nonlinear interaction wherein the reflected solitary wave follows a phase trajectory, asymptotically far from the wall, characterized by a velocity less than that of the incoming wave. In the figure are shown: t_a, the attachment time at which the incident wave crest arrives at the vertical wall; t_0, the time of maximum run-up at the wall; and t_d, the detachment time at which the wave crest leaves the wall. Fenton & Rienecker (1982) introduced t_l, the phase lag time, a measure of the temporal phase change incurred as a result of wall reflection. As seen in figure 1, this quantity expresses how much longer the wave crest remains against the wall than if it had been instantaneously reflected. The difficulty with using t_l is that it necessitates an accurate determination, either numerically or experimentally, of trajectory slopes at large distances from the wall after reflection. We propose using the wall residence time $t_r = t_d - t_a$ as an alternative measure of the effect of the wall on the wave. The time t_r is non-zero in the linear theory for two equal but oppositely directed waves. The departure of t_r from that predicted by linear theory is a measure of the effect of nonlinearity on the reflection process. This quantity is easily computed numerically using modern computational techniques. Moreover, measurement of the wall residence time should not pose any serious problem for the experimentalist, and dissipation effects during the short interaction period are expected to be minimal.

Temperville (1979) was the first to report the leading-order asymptotic formula for the wall residence time, using Lagrangian coordinates. His results were independently confirmed in an Eulerian framework by Power & Chwang (1984). At lowest order, the interaction between two solitary waves can be described by the linear superposition of two Korteweg–de Vries solitary waves of equal amplitude propagating in opposite directions (Byatt-Smith 1971). The resulting wall residence time may be written in the form

$$\frac{t_r}{\tau} = \frac{2}{\sqrt{3}} \ln\left(\frac{\sqrt{3}+1}{\sqrt{3}-1}\right) \epsilon^{-1/2} + O(\epsilon^{1/2}), \tag{3.1}$$

where time is made dimensionless with respect to $\tau = (h/g)^{1/2}$. Equation (3.1) shows that $t_r \to \infty$ as $\epsilon \to 0$, a feature stemming from the fact that the effective length of the wave increases to infinity in this limit.

Higher-order corrections to (3.1) may be found using the results of SM who computed the interaction waveform for two waves in head-on collision to $O(\epsilon^3)$. The interaction waveform $\zeta(\xi, \eta)$ is reported as equation (50) in their paper in terms of phase variables $\xi(x, t)$ for right-running and $\eta(x, t)$ for left-running waves given by their equations (53) and (54), respectively. It has been observed (Byatt-Smith 1988) that the

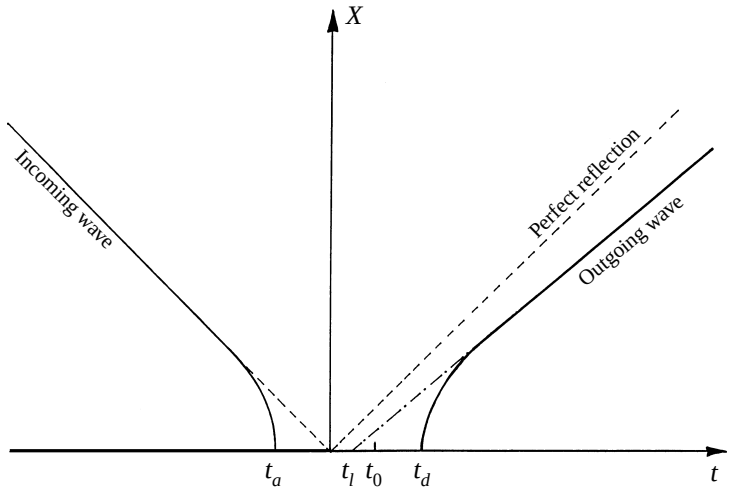

FIGURE 1. Schematic diagram of the incoming and outgoing wave crest trajectory for a large-amplitude wave showing the attachment time t_a, the lag time t_l, the time of maximum run-up t_0, and the detachment time t_d.

perturbation expansion is not uniformly valid for large time – hence SM's results must be interpreted with caution. The time origin for these mathematical calculations is the time of perfect reflection shown in figure 1.

To see whether our numerical computations are in agreement with asymptotic trends, we calculate only leading-order and first corrections to the time and amplitudes of wave attachment, detachment and maximum collision amplitude. The interaction waveform for two waves of equal amplitude ϵ in head-on collision given by SM, correct to $O(\epsilon^2)$, may be written

$$\zeta(\xi,\eta) = (S_1^2+S_2^2)\,\epsilon + [-\tfrac{3}{4}(S_1^2+S_2^2)+\tfrac{3}{4}(S_1^4+S_2^4)+\tfrac{1}{2}S_1^2\,S_2^2]\,\epsilon^2, \tag{3.2}$$

where here, and in what follows,

$$S_1 = \operatorname{sech}(\xi/2), \quad S_2 = \operatorname{sech}(\eta/2), \quad T_1 = \tanh(\xi/2), \quad T_2 = \tanh(\eta/2). \tag{3.3}$$

Defining the linear phase speed $c_0 = (gh)^{1/2}$ and introducing the constants $\alpha = \sqrt{3}/2h$ and $\beta = h/4\sqrt{3}$, the phase variables in (3.2) are given by

$$\frac{\xi(x,t)}{2\alpha} = (x-c_0\,t)\,\epsilon^{1/2}+2\beta(T_2+1)\,\epsilon-(\tfrac{5}{8}x-\tfrac{1}{8}c_0\,t)\,\epsilon^{3/2}+O(\epsilon^2), \tag{3.4a}$$

$$\frac{\eta(x,t)}{2\alpha} = (x+c_0\,t)\,\epsilon^{1/2}+2\beta(T_1-1)\,\epsilon-(\tfrac{5}{8}x+\tfrac{1}{8}c_0\,t)\,\epsilon^{3/2}+O(\epsilon^2), \tag{3.4b}$$

The location $x = 0$ of mid-interaction in this formulation may be considered as the position of a vertical boundary for solitary wave reflection. We will make use of the fact that at the wall the phase variables satisfy the symmetry relation $\xi(0,t) = -\eta(0,t)$. The attachment and detachment times are found by determining when the curvature of the free surface at the waterline changes from negative to positive, i.e. when the second partial x-derivative of ζ vanishes. Denoting $\mathrm{D} = \partial/\partial x$ we find the x-derivative of (3.2) at $x = 0$:

$$\mathrm{D}\zeta = -2S_1^2\,T_1\,\mathrm{D}(\xi/2)\,[\epsilon+\mu_1\,\epsilon^2]-2S_2^2\,T_2\,\mathrm{D}(\eta/2)\,[\epsilon+\mu_2\,\epsilon^2], \tag{3.5}$$

where

$$\mu_1 = -\tfrac{3}{4}+\tfrac{3}{2}S_1^2+\tfrac{1}{2}S_2^2, \quad \mu_2 = -\tfrac{3}{4}+\tfrac{3}{2}S_2^2+\tfrac{1}{2}S_1^2. \tag{3.6}$$

Differentiating (3.4*a*, *b*) yields

$$\mathrm{D}(\xi/2) = \alpha[\epsilon^{1/2} + \delta_1 \epsilon^{3/2}], \quad \mathrm{D}(\eta/2) = \alpha[\epsilon^{1/2} + \delta_2 \epsilon^{3/2}], \tag{3.7}$$

where

$$\delta_1 = \tfrac{1}{4}S_2^2 - \tfrac{5}{8}, \quad \delta_2 = \tfrac{1}{4}S_1^2 - \tfrac{5}{8}, \tag{3.8}$$

and hence (3.5) becomes

$$\mathrm{D}\zeta = -2\alpha(S_1^2 T_1 + S_2^2 T_2)\epsilon^{3/2} - 2\alpha[S_1^2 T_1(\mu_1 + \delta_1) + S_2^2 T_2(\mu_2 + \delta_2)]\epsilon^{5/2}. \tag{3.9}$$

We are interested in the solution of $\mathrm{D}^2\zeta = 0$ evaluated at the wall, where $x = 0$. If $x = 0$ then $T_1[\xi(0,t)] = -T_2[\eta(0,t)]$ for all t. A straightforward calculation yields

$$\mathrm{D}\zeta = -2\alpha\epsilon^{3/2}(T_1 + T_2)[1 - T_1^2 + T_1 T_2 - T_2^2 + \epsilon\tfrac{1}{8}\{7 - 19(T_1^2 + T_2^2) + 13T_1 T_2 + 18T_1^2 T_2^2 + 12(T_1^4 - T_1^3 T_2 - T_1 T_2^3 + T_2^4)\}].$$

in which it is implied that the arguments of T_1 and T_2 are evaluated at $x = 0$. The factor $(T_1 + T_2)$ is always zero at the wall owing to the symmetry of the interaction for equal-amplitude waves. $\mathrm{D}^2\zeta$ vanishes when the factor in square brackets vanishes. So setting this factor equal to zero, and putting $T_1 = -T_2$, gives an equation which will implicitly determine the times of attachment and detachment:

$$1 - 3T_2^2 + \epsilon\tfrac{1}{8}(7 - 51T_2^2 + 66T_2^4) = 0. \tag{3.10}$$

Expanding the nested expressions $T_2 = T_2(T_1(T_2 \ldots))$ to sufficiently high order, with the repeated use of 3.4(*a*, *b*), ultimately yields the following explicit expressions:

$$\frac{t_a}{\tau} = \frac{2}{\sqrt{3}}[-\kappa_0 \epsilon^{-1/2} + \tfrac{1}{8}(2 - \kappa_0)\epsilon^{1/2}], \quad \frac{t_d}{\tau} = \frac{2}{\sqrt{3}}[+\kappa_0 \epsilon^{-1/2} + \tfrac{1}{8}(2 + \kappa_0)\epsilon^{1/2}], \tag{3.11a, b}$$

where $\kappa_0 = \tanh^{-1}(1/\sqrt{3})$ and the subscripts denote attachment and detachment, respectively. Note that $t_d = -t_a$ at leading order and the residence time t_r is in accord with the result (3.1) given by Temperville (1979), Power & Chwang (1984), and Cooker (1990). At higher orders the attachment and detachment times are no longer antisymmetric about $t = 0$.

The amplitude of the waves at attachment and detachment found by inserting (3.11) into (3.2) and carrying out the expansions, are given by

$$\frac{\zeta_a}{h} = \tfrac{4}{3}\epsilon + \tfrac{1}{9}[\sqrt{3}(2 - \kappa_0) - 1]\epsilon^2, \quad \frac{\zeta_d}{h} = \tfrac{4}{3}\epsilon - \tfrac{1}{9}[\sqrt{3}(2 + \kappa_0) - 1]\epsilon^2. \tag{3.12a, b}$$

At lowest order the attachment and detachment amplitudes are the same, but this symmetry is broken at $O(\epsilon^2)$.

3.2. *Maximum run-up*

An asymptotic result for the time t_0 at which the water level at the wall reaches its maximum value ζ_0 is determined as follows. The condition for maximum run-up is that $S_1 = S_2 = 1$ simultaneously at the wall, a condition guaranteed if the arguments $\xi(0,t) = -\eta(0,t)$ are zero. In order to obtain non-trivial leading-order and first correction results, we must use the highest-order phase variable results of SM. Setting $x = 0$ in the $O(\epsilon^{5/2})$ result for ξ in equation (53) of SM leads to the equation

$$-\hat{t}_0 \epsilon^{1/2} + 2\alpha\beta(T_2 + 1)\epsilon + \tfrac{1}{8}\hat{t}_0 \epsilon^{3/2} + \beta(18S_1^2(T_2 + 1) - \tfrac{13}{2}T_2 - T_2^3 - \tfrac{15}{2})\epsilon^2 - \tfrac{59}{640}\hat{t}_0 \epsilon^{5/2} = 0, \tag{3.13}$$

implicitly determining the maximum run-up time $\hat{t}_0 = \alpha c_0 t_0$. Expanding the nested terms $T_2[\zeta(0,t)]$ with the aid of (3.4*b*) for small ϵ one obtains the explicit equation

$$-\hat{t}_0 \epsilon^{1/2} + \tfrac{1}{4}\epsilon + \tfrac{3}{8}\hat{t}_0 \epsilon^{3/2} + \tfrac{5}{4}\epsilon^2 + \left(\tfrac{801}{640}\hat{t}_0 + \tfrac{1}{12}\hat{t}_0^3\right)\epsilon^{5/2} = 0. \tag{3.14}$$

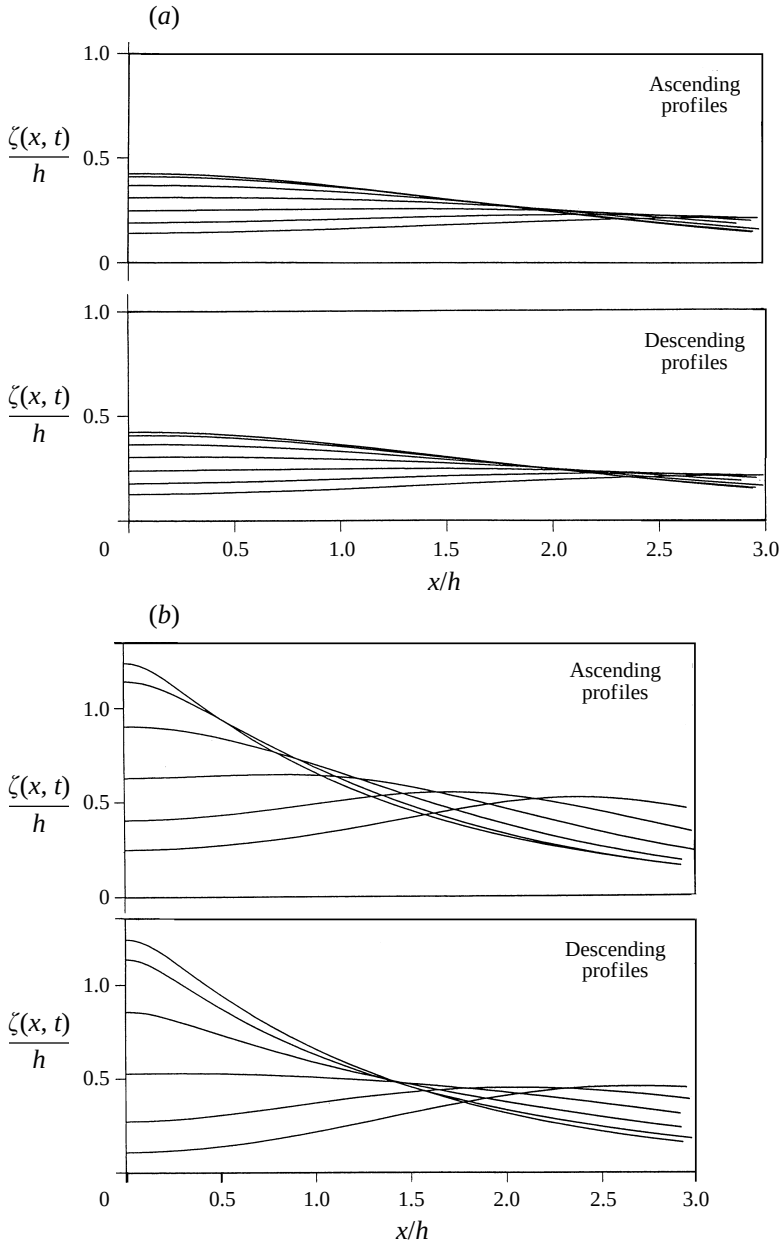

FIGURE 2. Free surface profiles for the fully nonlinear potential flow code for incoming and outgoing waves for (*a*) $\epsilon = 0.2$, and (*b*) $\epsilon = 0.5$. The time between successive profiles is $\tau/2$. The horizontal and vertical scales are equal. The free surface at maximum run-up is shown.

Assuming a series solution for $\hat{t}_0$ in powers of $\epsilon^{n/2}$ and inserting into (3.14) yields equations for the unknown coefficients at each order. Solution of these equations furnishes the maximum run-up time

$$\frac{t_0}{\tau} = \frac{1}{2\sqrt{3}}(\epsilon^{1/2} + \tfrac{43}{8}\epsilon^{3/2}) + o(\epsilon^2). \tag{3.15}$$

Thus t_0 always occurs later than the instant $t = 0$ predicted by a linear superposition

of the wave and its image. Insertion of (3.15) into (3.2) gives the maximum run-up amplitude correct to $O(\epsilon^2)$ as in (1.1*a*).

3.3. *Phase speed at impact*

Both experiment and numerical calculations show that the phase trajectories of both the incident and reflected waves are very steep near the wall. Maxworthy (1976) observed this feature in spite of the paucity of experimental data in the near-wall region. Well-resolved numerical simulations by Mirie & Su (1982), Fenton & Rienecker (1982), Grilli & Svendsen (1990), and Cooker (1990) suggest possibly infinite instantaneous phase speeds at the wall. Fenton & Rienecker write that the incident wave crest 'snaps through' to the wall.

The slope of the trajectory at the wall may be determined using (3.9) for the wave crest position $x_c(t)$. To leading order the position of the wave crest is given by the second root in

$$S_1^2 T_1 + S_2^2 T_2 = (T_1 + T_2)[1 + T_1 T_2 - T_1^2 - T_2^2] = 0. \tag{3.16}$$

The implicit transcendental relation determining the position $x_c(t)$ of the incoming $(x \geqslant 0, t < 0)$ wave is obtained using the positive root of the quadratic in square brackets, namely

$$T_1 = \tfrac{1}{2}(T_2 + (4 - 3T_2^2)^{1/2}). \tag{3.17}$$

Taking the time derivative of (3.17) gives the phase speed for an incoming wave

$$\dot{x}_c = c_0 \left[\frac{S_1^2(2T_1 - T_2) - S_2^2(2T_2 - T_1)}{S_1^2(2T_1 - T_2) + S_2^2(2T_2 - T_1)} \right], \tag{3.18}$$

in which the arguments $\{k(x_c(t) + ct)\}$ of the hyperbolic functions are found by solution of (3.17). As the wave approaches the wall $x_c \to 0$ and $t \to t_a$ which gives $S_1^2 = S_2^2$ and $T_2 = -T_1$. Thus the phase speed as the wave impacts the wall is given by

$$\dot{x}_c = c_0 \left[\frac{3T_1 - 3T_2}{T_1 + T_2} \right] \to \infty \quad \text{as} \quad T_2 \to -T_1. \tag{3.19}$$

An identical result is obtained for the outgoing trajectory obtained using the negative radical in (3.17) valid for $(x \geqslant 0, t > 0)$. Thus the phase velocities $\dot{x}_c$ for both the incident and reflected waves are infinite at the wall at lowest order in the perturbation formulation. Analysis of the equations describing the first correction to this result shows that crest speeds at attachment and detachment are finite and unequal.

4. Results

4.1. *Numerical calculations and asymptotic results*

The asymptotic results of Byatt-Smith (1988) for small-amplitude waves, and the work presented in §3, suggest that reflection is not symmetric. We can safely infer that the reflection process for *high*-amplitude waves is also not symmetric in time. At distances asymptotically far from the wall the incident wave is a pure solitary wave, and the reflected disturbance is a solitary wave of smaller amplitude followed by a dispersive tail. The asymmetry of the reflection process is also evident in the critical times t_a, t_d, and t_0, previously defined, and in t_m, the time of maximum instantaneous force. The sequence of events during reflection, which we have gleaned from the numerical solutions, is as follows. The wave approaches the wall and the waterline rises. When the crest is less than about $2h$ from the wall the crest accelerates. At the instant t_a the crest of the wave has 'snapped through' to the wall with a corresponding elevation ζ_a. During this period the force on the wall has its first and foremost maximum, at time t_m. For $\epsilon < 0.3$, $t_m \approx t_0$ and the force is mainly due to hydrostatic pressure. For

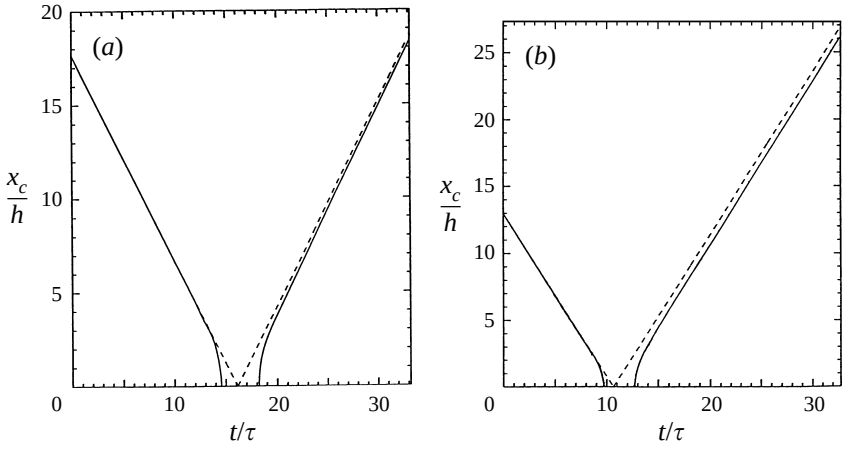

FIGURE 3. Wave trajectories computed for (*a*) $\epsilon = 0.2$ and (*b*) $\epsilon = 0.5$.

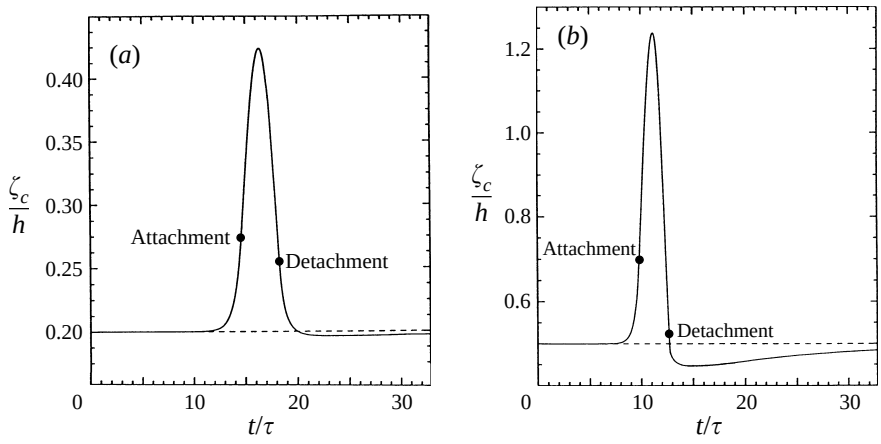

FIGURE 4. Wave crest amplitude as a function of time computed for (*a*) $\epsilon = 0.2$ and (*b*) $\epsilon = 0.5$ using the numerical code. Attachment and detachment points are indicated.

$\epsilon > 0.3$, however, the force maximum occurs while the waterline is still rising and a second smaller force maximum evolves during run-down. Lastly, the waterline detaches at t_d with an elevation ζ_d always less than ζ_a. A characteristic feature of the interaction is that the waterline at the wall spends more time falling than rising, i.e. $(t_0 - t_a) < (t_d - t_0)$.

Wave interaction profiles computed using the boundary-integral method for a low-amplitude wave $\epsilon = 0.2$ and a moderately high-amplitude wave $\epsilon = 0.5$ are presented in figures 2(*a*) and 2(*b*), respectively. Time is measured relative to the start of the computation for a solitary wave placed at distance x_0 from the wall. The corresponding wave crest trajectories are plotted in figures 3(*a*) and 3(*b*). In each case the wave propagates along a nearly straight trajectory until, near $x/h \approx 2$, it rapidly accelerates and attaches to the wall. At the end of the time that the crest is in residence at the wall, the crest leaves the wall at very high speed, but immediately decelerates into an almost straight trajectory nearly parallel to the trajectory formed by perfect reflection of the incident wave. In each case the phase shift continuously decreases as the wave moves away from the wall, but it is difficult to determine its final state. A much more sensitive measure of wave evolution is provided by the amplitude plots in figures 4(*a*) and 4(*b*).

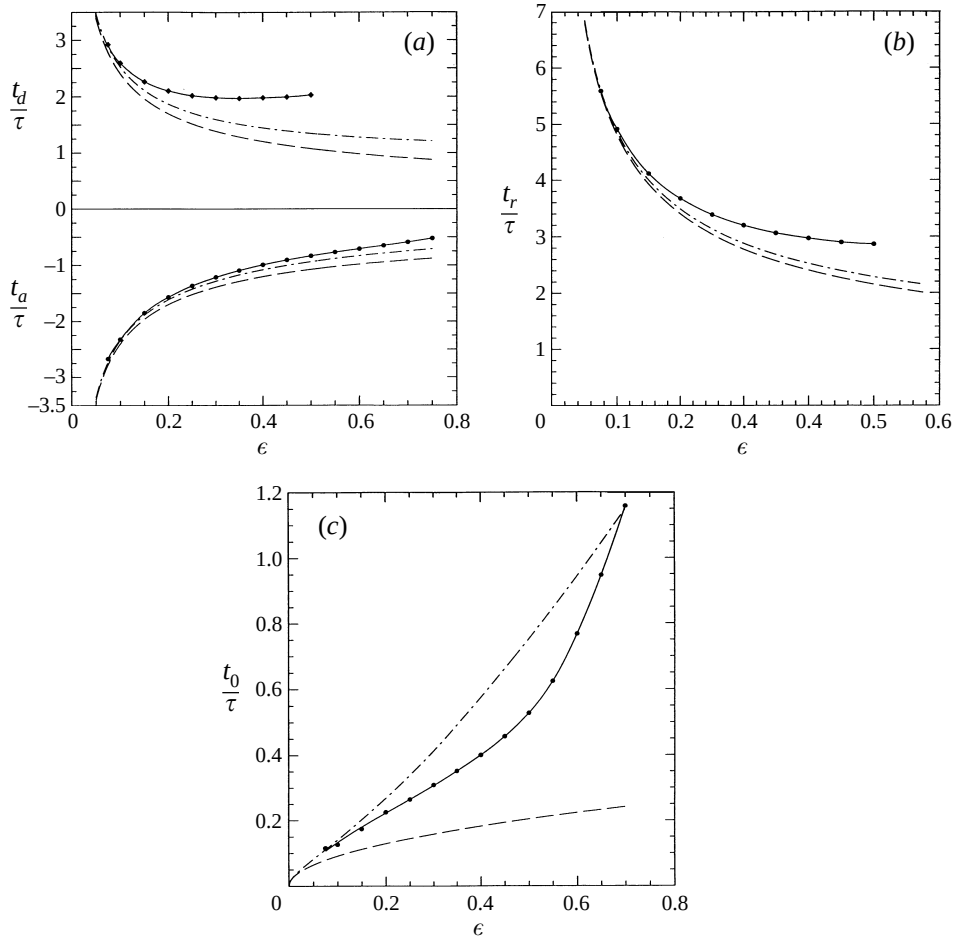

FIGURE 5. (*a*) Attachment and detachment times as a function of incident wave amplitude: —●—, attachment and —◆—, detachment numerical results; – – –, $O(\epsilon^{-1/2})$; –·–·–, $O(\epsilon^{1/2})$ asymptotics determined using the results of SM. (*b*) Wall residence time as a function of incident wave amplitude: —●—, numerical results; – – –, $O(\epsilon^{-1/2})$; –·–·–, $O(\epsilon^{1/2})$ asymptotics determined from the perturbation results of SM. (*c*) Time at maximum run-up as a function of incident wave amplitude: —●—, numerical results; – – –, $O(\epsilon^{1/2})$; –·–·–, $O(\epsilon^{3/2})$ asymptotics determined from the perturbation results of SM. The time origin in each of (*a–c*) is the mathematical centre of perfect reflection.

Both the small- and moderate-amplitude wave crests are still in a stage of adjustment at $t/\tau = 30$. Owing to the finite domain of the calculations, the evolution of the primary wave crest asymptotically far from the wall cannot be determined. Nonetheless, there is evidence of larger attenuation of the reflected wave for $\epsilon = 0.5$ than for $\epsilon = 0.2$ (note the different vertical scales in figures 4(*a*) and 4(*b*)).

Numerically determined attachment, detachment, and maximum run-up times are compared with asymptotic results in figure 5. The mathematical origin for the numerical computations was determined by projecting the trajectories of the incident waves to the wall as indicated by the dashed line in figure 1, using the release points x_0 and the numerically calculated nonlinear phase speeds c listed in table 1. The computed values of t_a, t_d, t_r, t_0 and ζ_0 are listed in table 2. Numerical results for t_a and t_0 are given up to $\epsilon = 0.7$; the program fails at $\epsilon = 0.75$ because of its inability to describe the neighbourhood of the waterline, which is an ascending narrow jet.

		$c/(gh)^{1/2}$	
ϵ	x_0/h	Numerical	Exact
0.075	20.624	1.0362	1.0361
0.100	22.609	1.0478	1.0480
0.150	17.395	1.0717	1.0717
0.200	16.166	1.0944	1.0943
0.250	15.100	1.1163	1.1163
0.300	19.558	1.1376	1.1375
0.350	13.642	1.1581	1.1581
0.400	14.558	1.1781	1.1781
0.450	12.737	1.1973	1.1973
0.500	12.958	1.2158	1.2158
0.550	11.994	1.2334	1.2334
0.600	12.402	1.2500	1.2500
0.650	11.751	1.2653	1.2653
0.700	11.554	1.2789	1.2789

TABLE 1. Release points and numerically calculated phase speeds for various wave amplitudes

ϵ	t_a/τ	t_d/τ	t_r/τ	t_0/τ	ζ_0/h
0.075	−2.792	2.801	5.593	0.1157	0.1530
0.100	−2.448	2.468	4.916	0.1265	0.2055
0.150	−2.027	2.089	4.116	0.1741	0.3130
0.200	−1.789	1.883	3.672	0.2252	0.4241
0.250	−1.629	1.758	3.387	0.2642	0.5395
0.300	−1.521	1.676	3.197	0.3087	0.6602
0.350	−1.444	1.617	3.061	0.3519	0.7875
0.400	−1.393	1.577	2.970	0.4008	0.9237
0.450	−1.364	1.536	2.900	0.4569	1.0721
0.500	−1.362	1.505	2.867	0.5280	1.2384
0.550	−1.394	—	—	0.6248	1.4320
0.600	−1.474	—	—	0.7584	1.6677
0.650	−1.597	—	—	0.9474	1.9606
0.700	−1.756	—	—	1.1584	2.3279

TABLE 2. Computed values of t_a, t_d, t_r, t_0 and ζ_0 for various wave amplitudes

Numerical results for t_d are given only up to $\epsilon = 0.50$; at $\epsilon = 0.55$ the program becomes unstable as the instant of detachment is approached. Figure 5(*a*) exhibits the variation of attachment and detachment times with ϵ. Plots of the wall residence time and the time at maximum run-up are given in figures 5(*b*) and 5(*c*), respectively. In each figure the improved asymptotics tend favourably toward the numerical computations. However, the useful range of convergence of the asymptotics in figure 5(*c*) is very limited.

Figure 6(*a*) displays the numerical computations and asymptotic results for the wave amplitudes at attachment and detachment. Note that the equal-amplitude symmetry of the asymptotics at $O(\epsilon)$ is broken at $O(\epsilon^2)$, and that these highest-order results closely conform to the numerical trends. In figure 6(*b*) the maximum run-up computations are compared with SM's prediction given by (1.2*a*) and with the numerical results of Fenton & Rienecker (1982). With the exception of a single point near $\epsilon = 0.45$, the numerical values reported by Fenton & Rienecker (1982) are in excellent agreement with the present computations.

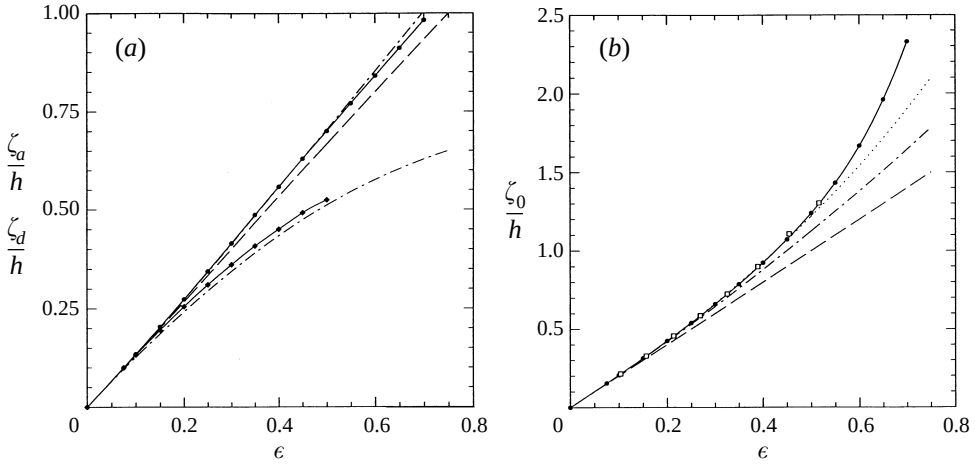

FIGURE 6. (*a*) Attachment and detachment amplitudes as functions of incident wave height, ϵ. Numerical results: —●—, attachment; —◆—, detachment. Asymptotics determined from the perturbation results of SM: – – –, $O(\epsilon^{-1/2})$; –·–·, $O(\epsilon^{1/2})$. Note that at $O(\epsilon^{-1/2})$ the attachment and detachment amplitudes are predicted to be equal. (*b*) Maximum run-up: —●—, numerical results; —◇—, calculations of Fenton & Rienecker (1982); – – –, $O(\epsilon)$: –·–·, $O(\epsilon^2)$: · · · ·, $O(\epsilon^3)$ results of SM.

Figure 7(*a*) gives the instantaneous wall force, F_w, as a function of time relative to t_0, for selected values of ϵ obtained from the fully nonlinear potential flow code. Note that the single maximum for $\epsilon < 0.3$ becomes a double maximum in the vicinity of $\epsilon = 0.4$. The force peak occurs before maximum run-up because the upsurging wave forms a narrow jet. Figure 7(*b*) gives the maximum instantaneous force $(F_w)_m$, as a function of ϵ, as computed here and by Fenton & Rienecker (1982): note that our results include much higher waves than the previous work. For $\epsilon = 0.5$ Grilli & Svendsen (1990) found $(F_w)_m = 1.52\rho gh^2$, which agrees with our value at this level of ϵ.

4.2. *Comparison with experiment*

In Maxworthy's (1976) measurements of solitary wave interactions, data were taken from 8 mm cine film shot at 64 frames/s. We analyse one roll of the cine film made available to us which documents 19 sequences of wave reflection at a vertical wall in a lucite channel nominally 5 m in length with rectangular section 20 cm wide by 30 cm high. As mentioned in the Introduction, the waves were produced manually in an effort to obtain a single solitary wave. Segur (1973) has shown that a sufficiently large compact initial disturbance will evolve into one or more solitary waves followed by a dispersive tail. Careful viewing of the original film strip showed that many of the incident waves were followed by a long, much smaller-amplitude wave that could have been either the beginning of a dispersive tail or a second coherent solitary wave.

Backlighting through diffusive white paper and red colouring added to the water permitted Maxworthy to obtain good definition of the free surface. The camera was positioned some distance upstream of the endwall to record sufficient data to define the incoming and outgoing trajectory of the primary disturbance. This placed the reflecting boundary at the extreme edge of the field of view where the lighting was somewhat diminished. For this reason the film strip was analysed on a Rank Cintell MK IIIC enhanced cine film viewing system with $x-y$ zooming and variable video level. Measurements of the instants of wave attachment, maximum wave run-up, and wave detachment were made by locating the frame nearest to the event with an estimated error of ± 1 frame. A separate stop-action film projector was used to extract amplitude

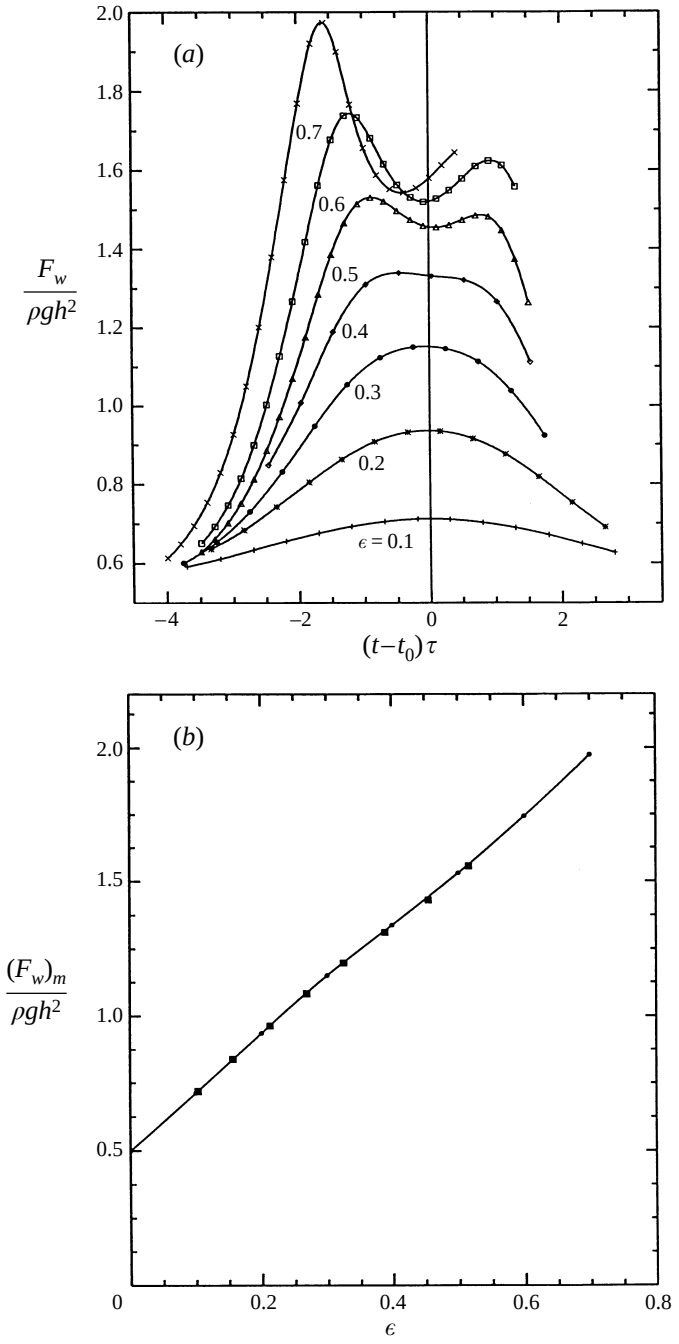

FIGURE 7. (*a*) Instantaneous wall force computed using the numerical code plotted for selected values of wave amplitude. (*b*) Maximum instantaneous wall force plotted against wave amplitude: —●—, present calculations; —◆—, numerical results of Fenton & Rienecker (1982).

measurements of the incident wave in the middle of the field of view, some one to three wavelengths upstream of the endwall, depending on the incident wave amplitude. No calibrated length scale was in the field of view, but fortunately the top of the lucite

Run	h (cm)	$h+a$ (cm)	ϵ	$\frac{t_a-t_0}{\tau}$	$\frac{t_d-t_0}{\tau}$	$\frac{t_r}{\tau}$
1	4.915	5.829	0.186	−1.765	1.986	3.751
2	4.915	5.944	0.209	−1.765	1.956	3.751
3	4.896	7.315	0.488	−1.326	1.547	2.874
4	4.915	5.486	0.116	−2.206	2.427	4.633
5	4.915	6.706	0.364	−1.324	1.765	3.089
6	4.915	6.401	0.302	−1.544	1.544	3.089
7	4.915	7.010	0.426	−1.324	1.544	2.868
8	4.953	5.791	0.169	−1.758	1.978	3.736
9	4.953	7.087	0.442	−1.319	1.758	3.077
10	4.915	5.944	0.209	−1.765	1.765	3.530
11	4.915	6.058	0.233	−1.765	1.765	3.530
12	4.915	7.125	0.449	−1.324	1.544	2.868
13	4.915	7.391	0.504	−1.324	1.544	2.868
14	4.915	5.906	0.202	−1.765	1.764	3.530
15	4.915	6.553	0.333	−1.544	1.544	3.089
16	4.953	7.239	0.462	−1.319	1.758	3.077
17	4.915	6.096	0.240	−1.765	1.765	3.530
18	4.915	6.896	0.403	−1.544	1.544	3.089
19	4.915	6.668	0.357	−1.544	1.544	3.089

TABLE 3. Measurements of the 19 wave reflections taken from Maxworthy's cine film of his 1976 experiment.

channel was visible in every frame. This 40.38 cm dimension provided an accurate† reference from which measurements of the quiescent water level h and incident peak wave elevation a could be made from an enlarged projection of the film onto a white plastic surface.

Measurements of the 19 wave reflections were taken, with results given in table 3. The experiments were all conducted with the same fluid volume having average measured fluid depth $h = 4.92$ cm. The gravitational constant was taken to be 980 cm s^2 and we note that only time differences $t_a - t_0$, $t_d - t_0$ and $t_d - t_a$ can be measured. Dimensionless plots of the first two quantities are given in figure 8(*a*) and compared with our numerical computations. The experimental error bars represent ± 0.22 dimensionless time units corresponding to the $\pm 1/64$ s estimated error in locating the critical times. The numerical and experimental wall residence times are compared in figure 8(*b*).

5. Discussion and conclusions

When a large-amplitude solitary wave collides with a vertical wall numerical results and perturbation methods have already shown that the reflected wave is different from its incident state. After reflection the solitary wave loses energy to a dispersive wave train and loses height, so ultimately the speed of the reflected wave is smaller than before collision. This observation shows that even within the confines of an inviscid fluid model the so-called phase shift of a reflected solitary water wave is spatially dependent. We have concentrated on examining the fluid flow in the neighbourhood of the wall in order to determine details of the collision in this circumstance. In particular, in the absence of a constant phase shift for large-amplitude incident waves, we have computed the wall residence time which we put forth as an alternative measure of the

† We are indebted to Dr G. R. Spedding for providing us the measurement of the channel height.

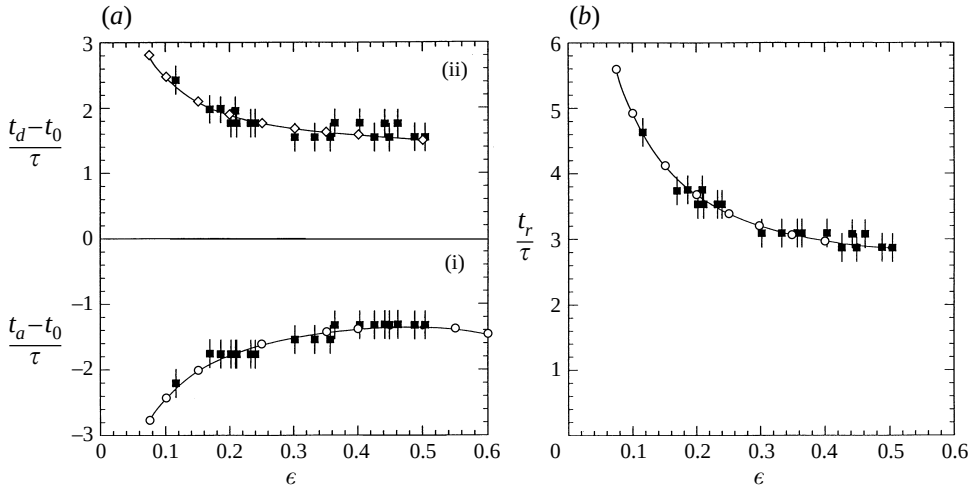

FIGURE 8. (*a*) A comparison of the attachment and detachment times taken from Maxworthy's (1976) measurements (■) with our numerically determined values (—○—). The error bars are $\pm 1/64$ s. Time increases up the page and $t = 0$ corresponds to the instant of maximum run-up. (i) The instant of attachment, (ii) the instant of detachment, as a function of ϵ. (*b*) A comparison of measurements of the wall residence time taken from the cine film of Maxworthy (1976) with numerically determined values. Symbols as for (*a*).

effect of wall–wave interaction. The numerical results show that once the wave crest becomes attached to the wall, it spends less time ascending to maximum run-up than it does descending to detachment, i.e. $(t_0 - t_a) < (t_d - t_0)$. The wall residence time is very long for waves of small amplitude, and we confirm numerically the result of Temperville (1979) that in the limit $\epsilon \to 0$, t_r is proportional to $\epsilon^{-1/2}$. However, increasing the height of the incident wave causes t_r to decrease to an approximately constant value of about 3τ, a numerical result verified by experiment in figure 8(*b*). There are two separate effects which contribute to t_r. The first is the geometric effect of linearly superposing two Korteweg–de Vries solitary waves. The second is a nonlinear effect in which a vertical jet takes time to ascend and descend the wall. In brief, small-amplitude solitary waves spend a long time at the wall, while high-amplitude waves create tall jets running up and down the wall during the nearly constant time period 3τ. Grilli & Svendsen (1990) found for $\epsilon = 0.5$ a time $t_r = 2.75\,(h/g)^{1/2}$ which agrees reasonably well with our computed value $t_r = 2.87\,(h/g)^{1/2}$.

The measurements of the time of run-up $(t_0 - t_a)$ and the time of run-down $(t_d - t_0)$ plotted in figure 8(*b*) are in accord with the numerical results over the available range of experimental wave amplitudes $0.12 < \epsilon < 0.50$. This may at first seem surprising in view of the fact that some of the incident waves were followed by a weak secondary wave or dispersive tail. The agreement between measurement and computation suggests that small-amplitude trailing waves did not appreciably interfere with the lead wave's collision with the endwall. It may therefore be concluded that the wall residence time t_r is a robust measure of the phase change that takes place during wave reflection.

The numerical computations and asymptotic results derived from the perturbation calculations of SM agree in two respects: first, the crest height at attachment is greater than at detachment and, secondly, the crest takes longer to descend the wall than to ascend it. Moreover, the numerically computed times of run-up and run-down are confirmed by experiment in figure 8(*a*). We note that carrying out the asymptotic calculations for attachment and detachment times to higher order gives a slight

improvement only for values of ϵ less than approximately 0.15. This small range of convergence is apparently due to the non-uniformity of the perturbation method, as pointed out by Byatt-Smith (1988).

Figure 6(*b*) verifies that the run-up ζ_0 for weakly nonlinear waves is more than twice the incident wave amplitude, in agreement with the original prediction of Byatt-Smith (1971). At sufficiently high amplitude, $\epsilon > 0.65$, the run-up is observed to exceed three times the incident wave amplitude. As shown in figure 7(*a*), for $\epsilon < 0.3$ the maximum force occurs at maximum run-up, and the pressure in the fluid is mostly hydrostatic. For $\epsilon > 0.4$ the numerical calculations show that the vertical acceleration of the fluid is significant, especially during the run-up phase of the collision. Also the fluid acceleration associated with the upward projection of the water increases the pressure near the wall above hydrostatic, and a first maximum occurs. After the vertical column of fluid comes nearly to rest it slides back down the wall under the restoring force of gravity. The fluid decelerates at the end of its descent and this is associated with another increase in the wall pressure above its hydrostatic value, and so brings about a second maximum in the force as a function of time, occuring after t_0 when ϵ is large. The maximum force in figure 7(*b*) is a remarkably linear function of wave amplitude up to $\epsilon = 0.7$ considering the asymmetry in the instantaneous wall force in figure 7(*a*).

The main findings of this paper are as follows. Since the phase shift of a large-amplitude solitary wave, reflecting from a vertical wall, is spatially dependent, these waves are not solitons. In view of the fact that a constant phase shift does not exist, we propose that a useful measure of phase changes incurred by the collision is the time spent by the wave crest in residence against the wall. The instants at which the crest attaches and detaches from the wall are well-defined and might be measured more accurately in future experiments. Measures of the time spent by the crest at the wall predicted numerically and measured experimentally are in accord. The computations show a marked asymmetry in the motion between run-up and run-down. The asymmetry partly explains the long-time behaviour of the reflected wave, which is unsteady and pursued by small surface disturbances in the form of a dispersive tail. The maximum run-up of the wave is in close agreement with previous studies, in particular with the results of Fenton & Rienecker (1982) computed using a Fourier method for solving the nonlinear wave problem. The force on the wall as a function of time has two maxima when the wave has an incident height greater than 0.4, as previously noted by Grilli & Svendsen (1990). The maximum force as a function of incident wave height is quite linear, an observation yet to be adequately explained on physical grounds. The waterline acceleration partly explains the increased pressures on the wall during run-up and run-down. The acceleration of the crest towards attachment onto the wall, and during detachment from the wall, is very large, in agreement with lowest-order perturbation theory which predicts infinite horizontal phase speed of the wave crest at attachment and detachment.

The authors are grateful to the University of East Anglia, UK for providing funds for a Visiting Fellowship for one of us (P.D.W.) during the study reported here. Stimulating discussions with Professor H. Segur are acknowledged. We are grateful to Professor T. Maxworthy for making available his original cine film of solitary wave reflections.

REFERENCES

Baker, G. R., Meiron, D. I. & Orszag, S. A. 1982 Generalised vortex methods for free-surface flow problems. *J. Fluid Mech.* **123**, 477–501.

Byatt-Smith, J. G. B. 1971 An integral equation for unsteady surface waves and a comment on the Boussinesq equation. *J. Fluid Mech.* **49**, 625–633.

Byatt-Smith, J. G. B. 1988 The reflection of a solitary wave by a vertical wall. *J. Fluid Mech.* **197**, 503–521.

Chan, R. K. C. & Street, R. L. 1970 A computer study of finite amplitude water waves. *J. Comput. Phys.* **6**, 68–94.

Cooker, M. J. 1990 The interaction between steep water waves and coastal structures. PhD thesis, University of Bristol, UK.

Dold, J. W. 1992 An efficient surface-integral algorithm applied to unsteady gravity waves. *J. Comput. Phys.* **103**, 90–115.

Dold, J. W. & Peregrine, D. H. 1986 An efficient boundary-integral method for steep unsteady water waves. In *Numerical Methods for Fluid Dynamics II* (ed. K. W. Morton & M. J. Baines), pp. 671–679. Oxford University Press.

Fenton, J. D. & Rienecker, M. M. 1982 A Fourier method for solving nonlinear water-wave problems: application to solitary-wave interactions. *J. Fluid Mech.* **118**, 411–443.

Grilli, S. & Svendsen, I. A. 1990 The propagation and runup of solitary waves on steep slopes. *CACR Rep.* 91-04. Department of Civil Engineering, University of Delaware.

Longuet-Higgins, M. S. & Cokelet, E. D. 1976 The deformation of steep surface waves on water. I. A numerical method of computation. *Proc. R. Soc. Lond.* A **350**, 1–26.

Maxworthy, T. 1976 Experiments on the collision between two solitary waves. *J. Fluid Mech.* **76**, 177–185.

Mirie, R. M. & Su, C. H. 1982 Collisions between two solitary waves. *J. Fluid Mech.* **115**, 475–492.

Oikawa, M. & Yajima, N. 1973 Interaction of solitary waves – a perturbation approach to nonlinear systems. *J. Phys. Soc. Japan* **34**, 1093–1099.

Power, H. & Chwang, A. T. 1984 On reflection of a planar solitary wave. *Wave Motion* **6**, 183–195.

Renouard, D. P., Seabra-Santos, F. J. & Temperville, A. M. 1985 Experimental study of the generation, damping and reflexion of a solitary wave. *Dyn. Atmos. Oceans* **9**, 341–358.

Segur, H. 1973 The Korteweg–de Vries equation and water waves. Solutions of the equation. Part 1. *J. Fluid Mech.* **59**, 721–736.

Su, C. H. & Gardner, C. S. 1969 Korteweg–de Vries equation and generalizations. III. Derivation of the Korteweg-de Vries equation and Burgers equation. *J. Math. Phys.* **10**, 536–539.

Su, C. H. & Mirie, R. M. 1980 On head-on collisions between two solitary waves. *J. Fluid. Mech.* **98**, 509–525 (referred to herein as SM).

Tanaka, M. 1986 The stability of solitary waves. *Phys. Fluids* **29**, 650–655.

Tanaka, M., Dold, J. W., Lewy, M. & Peregrine, D. H. 1987 Instability and breaking of a solitary wave. *J. Fluid Mech.* **185**, 235–248.

Temperville, A. 1979 Interactions of solitary waves in shallow water theory. *Arch. Mech.* **31**, 177–184.

Vinje, T. & Brevik, P. 1981 Numerical simulation of breaking waves. *Adv. Water Resources* **4**, 77–82.

Zabusky, N. J. & Kruskal, M. D. 1965 Interaction of 'solitons' in a collisionless plasma and the recurrence of initial states. *Phys. Rev. Lett.* **15**, 240–243.